instruments

MDPI

Article

FASER's Electromagnetic Calorimeter Test Beam Studies

Charlotte Cavanagh on behalf of the FASER Collaboration

Department of Physics, University of Liverpool, Liverpool L69 3BX, UK; charlotte.cavanagh@cern.ch

Abstract: FASER, or the Forward Search Experiment, is a new experiment at CERN designed to complement the LHC's ongoing physics program, extending its discovery potential to light and weakly interacting particles that may be produced copiously at the LHC in the far-forward region. New particles targeted by FASER, such as long-lived dark photons or axion-like particles, are characterised by a signature with two oppositely charged tracks or two photons in the multi-TeV range that emanate from a common vertex inside the detector. The full detector was successfully installed in March 2021 in an LHC side tunnel 480 m downstream from the interaction point in the ATLAS detector. FASER is planned to be operational for LHC Run 3. The experiment is composed of a silicon-strip tracking-based spectrometer using three dipole magnets with a 20 cm aperture, supplemented by four scintillator stations and an electromagnetic calorimeter. The FASER electromagnetic calorimeter is constructed from four spare LHCb calorimeter modules. The modules are of the Shashlik type with interleaved scintillator and lead plates that result in 25 radiation lengths and 1% energy resolution for TeV electromagnetic showers. In 2021, a test beam campaign was carried out using one of the CERN SPS beam lines to set up the calibration of the FASER calorimeter system in preparation for physics data taking. The relative calorimeter response to electrons with energies between 10 and 300 GeV, as well as high energy muons and pions, has been measured under various high voltage settings and beam positions. The measured calorimeter resolution, energy calibration, and particle identification capabilities are presented.

Keywords: resolution; calorimeter; pre-shower

Citation: Cavanagh, C., on behalf of the FASER Collaboration. FASER's Electromagnetic Calorimeter Test Beam Studies. *Instruments* **2022**, *6*, 31. https://doi.org/10.3390/instruments6030031

Academic Editors: Fabrizio Salvatore, Alessandro Cerri, Antonella De Santo and Iacopo Vivarelli

Received: 29 July 2022
Accepted: 26 August 2022
Published: 31 August 2022

Publisher's Note: MDPI stays neutral with regard to jurisdictional claims in published maps and institutional affiliations.

1. Introduction

There are many models to suggest new physics beyond the standard model (SM), for example, the possible existence of dark sectors (DS) that may contain new, light, weakly coupled particles that interact only very weakly with ordinary matter. FASER [1–3] is a new experiment designed to detect potentially long-lived particles (LLPs) produced at the ATLAS interaction point (IP1) in the forward region. It is located 480 m downstream of IP1 in the TI12 service tunnel. These particles are highly collimated, and their decay products have around TeV-scale energies.

The physics models targeted by FASER are characterised by the presence of LLPs, such as dark photons (A') and axion-like particles (ALPs, a). Dark photons [4] are hypothetical particles that belong to a DS and form a portal to the SM. This leads to a coupling between the SM and the DS, the strength of which is governed by a mixing parameter ϵ. The size of ϵ determines the strength of the interaction, hence the lifetime of the dark photon. Dark photons that have a mass $m_{A'}$ below a few hundred MeV predominantly decay into e^+e^- and $\mu^+\mu^-$ pairs. ALPs [4] are weakly interacting, pseudoscalar particles. In the photon-dominant case, there is a coupling $g_{a\gamma\gamma}$ between the SM and the ALP, a. The smaller this coupling, the more long-lived the particle. Identification of electrons, and photons in the case of ALPs, relies on energy deposits in the ECAL, hence FASER's main sensitivity in the low mass region is to e^+e^- pairs and $\gamma\gamma$ pairs resulting from dark photon decay and ALP decay, respectively. Figure 1 shows the decay mode, and the area of parameter space that FASER and the possible FASER2 upgrade will explore in the case of dark photons. Figure 2 shows the same for ALPs, in the photon-dominant case.

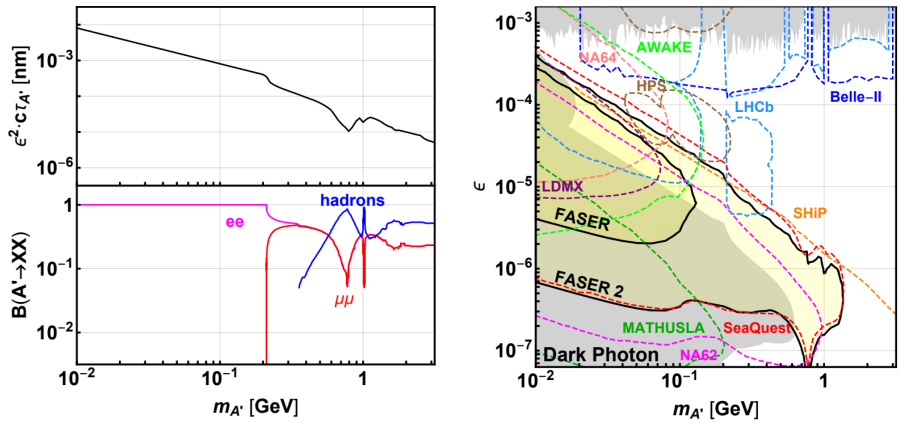

(**a**) (**b**)

Figure 1. (**a**) Dark photon decay modes according to mass range. (**b**) FASER and FASER2 (proposed, enlarged successor of FASER) accessible parameter space compared with current and proposed experiments [3].

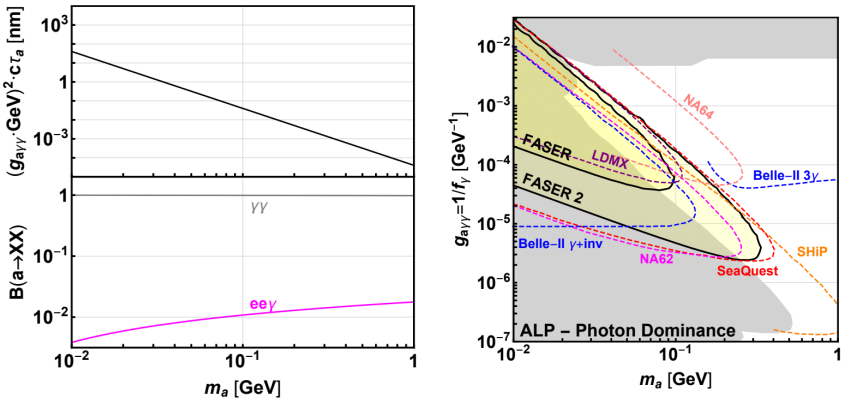

(**a**) (**b**)

Figure 2. (**a**) ALP decay modes according to mass range. (**b**) FASER and FASER2 accessible parameter space compared with current and proposed experiments [3].

2. The FASER Experiment

The main components of the FASER experiment are shown in Figure 3 [1]. A particle produced at IP1 enters FASERν, an emulsion detector made of tungsten plates that act as a target for neutrinos, interleaved with emulsion films to record the trajectories of charged particles. FASERν is followed by two scintillator veto stations that veto charged particles coming through the tunnel walls from IP1, primarily muons. The veto stations are followed by a 0.6 T permanent dipole magnet that also acts as a decay volume for incoming LLPs. It has a 10 cm aperture radius and is 1.5 m long. Next is the spectrometer which consists of two 1 m long 0.6 T dipole magnets. FASER has the IFT (interface tracker) in addition to three tracking stations, each made up of three layers of silicon strip detectors. These are located at either end of the dipole magnets, and one is in between. FASER uses ATLAS silicon trackers (SCT) modules [5]. The pre-shower station, the details of which are shown in Figure 4, is made up of two scintillators, each preceded by a 3 mm thick tungsten radiator in addition to 5 cm of graphite. The primary role of the pre-shower station is for particle identification (PID). Finally, FASER's electromagnetic calorimeter (ECAL), shown in Figure 5, is made of 4 LHCb ECAL modules [6]. These Shashlik-type calorimeter modules contain 66 alternating layers of 2 mm lead and 4 mm plastic scintillator plates, with a total of 25 radiation lengths. Between the lead and scintillator plates, there is a layer of TYVEC paper. A 10 dynode-stage head-on photo-multiplier tube (PMT) module provides a readout signal in the form of PMT pulses, as with the pre-shower station. The role of the calorimeter

is to measure the energy deposits made by the electrons and photons that result from the decay of the dark photons and ALPs.

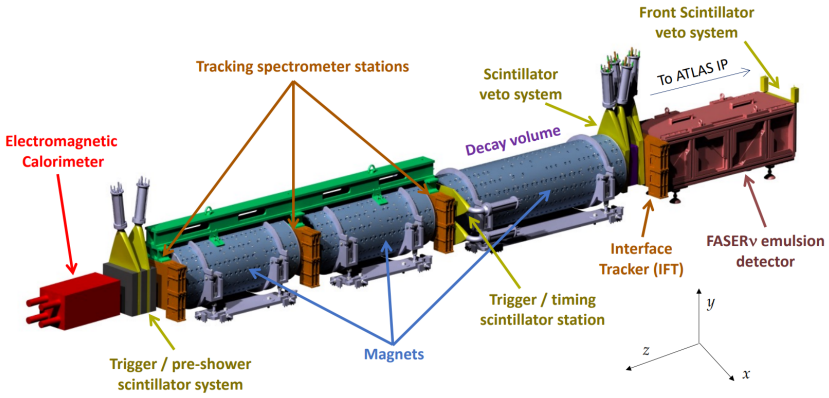

Figure 3. Diagram of FASER and FASERν components [1].

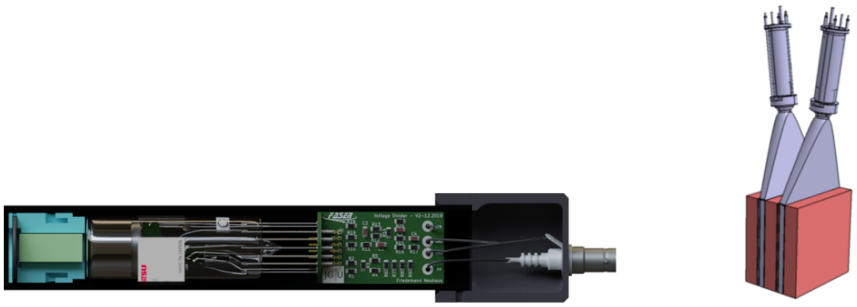

(**a**) (**b**)

Figure 4. (**a**) A diagram of a PMT module that provides readout pulses to the pre-shower station and calorimeter modules. (**b**) A sketch of the pre-shower station showing the two scintillators (grey), each preceded by 3 mm of tungsten and 5 cm of graphite (red).

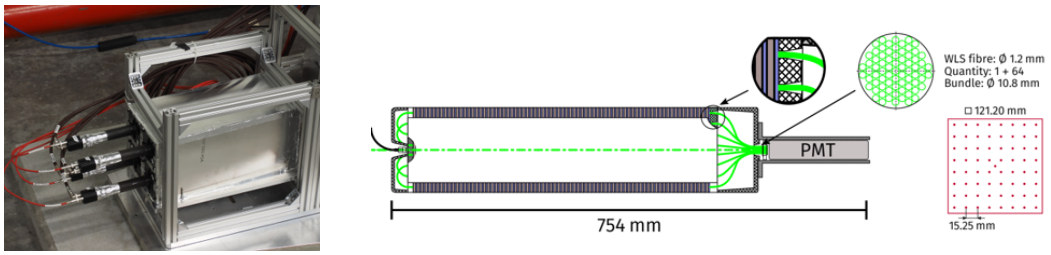

(**a**) (**b**)

Figure 5. (**a**) A photograph taken of the FASER ECAL in the TI12 tunnel, showing the 2 × 2 layout. (**b**) A diagram of the LHCb outer ECAL modules [6] used in FASER.

3. Results of the 2021 FASER Calorimeter Test Beam

3.1. Aims and Overview

The aims of the test beam were to calibrate the calorimeter modules using electron beams with energy between 10 and 300 GeV. Twenty-four positions across the modules' surface were scanned. In addition, the uniformity of the muon response was measured at 150 GeV, and a pion scan was performed at 200 GeV to study the hadronic response. Over 150 million events were recorded over the course of the test beam, primarily from the centre of the upper middle ECAL module. There were a number of runs performed under special conditions with the removal of the pre-shower material to study the resulting effects on energy (charge) deposited in the calorimeter.

The test beam was carried out at the CERN H2 beam line [7]. The test beam detector setup shown in Figure 6 consists of the trigger scintillator counter, the IFT station, the

pre-shower station, and the calorimeter. In the test beam, six calorimeter modules were used: the four intended to be installed in the TI12 tunnel, plus two spare modules arranged in a 3 × 2 configuration.

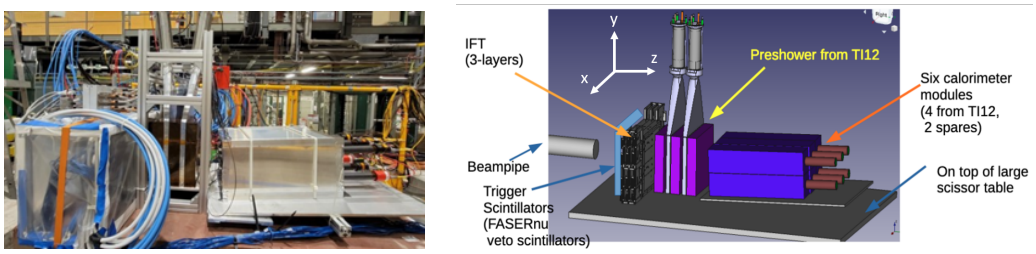

(**a**) (**b**)

Figure 6. (**a**) A photograph and (**b**) a diagram of the test beam setup, carried out in EHN1 (Experimental Hall North) at CERN. The coordinate system is defined in this figure.

3.2. Data Analysis

The PMT signals from the ECAL, pre-shower, and trigger scintillators are digitised at 500 MHz by 14-bit ADCs and read out in a wide window (1.2 µs), and the integrated charge is summed in a window around the expected peak signal. The readout for most events is triggered by signals in both trigger scintillators exceeding a predefined threshold at the same time. Besides the digitiser, hits in the tracker stations are read out in a 75 ns window and used to reconstruct tracks. The response of the calorimeter modules is studied using events selected as follows:

- The event trigger bit must indicate that the front two trigger scintillators were hit.
- Only one track must be found in the event, with tracks reconstructed according to a dedicated tracking algorithm.
- Tracks must be relatively straight with angle cuts such that the angular spread in the x and y plane is $\mid \theta_x \mid$ and $\mid \theta_y \mid < 2$ degrees.
- The track position must be within a 20 mm × 20 mm square area surrounding the beam position, obtained from extrapolating the track to the face of the calorimeter.

For each beam energy E, the resulting charge distribution deposited in the calorimeter is converted in terms of energy deposits and fitted to a crystal ball such that the energy resolution $\frac{\sigma_E}{E}$ can be obtained. Three terms contributed to the resolution according to the relation below:

$$\frac{\sigma_E}{E} = \frac{a}{\sqrt{E}} \oplus \frac{b}{E} \oplus c$$

where $\oplus$ indicates the quadratic sum. The $\frac{a}{\sqrt{E}}$ term is the stochastic term, $\frac{b}{E}$ is the noise term, and c is the constant term.

3.3. Test Beam Simulation

FASER's simulation is based on the Geant4 package [8]. LHCb test beam results using the same ECAL modules were used for comparison when building the simulation and studying the energy response and resolution, before it could be validated by FASER's own test beam data. At this stage, the simulation does not include any digitisation. Digitisation is a step which mimics the detector electrons by converting the simulation output into an output similar to the PMT pulses of real data. A dedicated geometry was developed for the test beam simulation. An example of an event display, produced based on ATLAS VP1 software [9], is shown in Figure 7 with the full test beam setup.

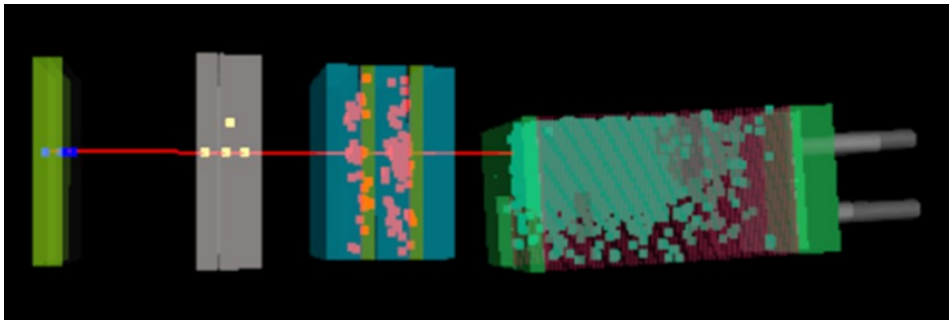

Figure 7. An event display of a simulated 100 GeV electron passing through the tracker station and the pre-shower station, before showering in the ECAL.

3.4. Pre-Shower Correction

The pre-shower "steals" a portion of the EM shower from the calorimeter, as a direct result of the two radiation lengths of the tungsten radiator. This effect varies on an event-by-event basis and thus degrades the energy resolution. This is corrected for in order to obtain the best energy resolution measurement. The total deposited charge in the pre-shower station compared to the total deposited charge in the calorimeter can be seen in Figure 8a for a 100 GeV electron.

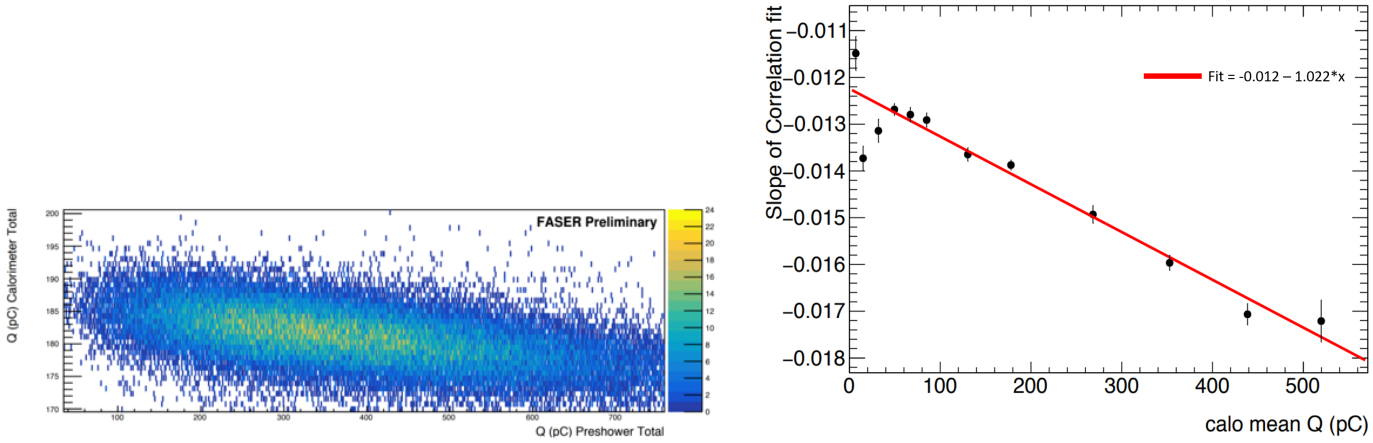

(**a**) (**b**)

Figure 8. (**a**) The deposited charge in the pre-shower versus calorimeter for 100 GeV electron. (**b**) The slope of correlation fit between charge deposits in the pre-shower and calorimeter, as a function of the mean deposited charge in the calorimeter for electrons with an incident beam energy of 10–300 GeV.

Studying the gradient of Figure 8a, compared to similar plots over the full electron energy range, the test beam data show a dependence on beam energy in terms of the fraction deposited in the pre-shower relative to the calorimeter. This dependence on beam energy is shown in Figure 8b, which demonstrates the correlation of charge deposits in the pre-shower versus the calorimeter for 10 GeV–300 GeV electrons, as a function of the mean charge deposited in the calorimeter. A pre-shower correction was derived to mimic the absence of a pre-shower station, taking into account the deposited charge in the calorimeter and pre-shower station:

$$Q_{corrected} = Q_{calo} + \left(m * Q_{pre-shower}\right),$$

where Q is the total deposited charge and m is the gradient derived from the fit in Figure 8b. The pre-shower correction aims to mimic the distribution of the deposited charge, seen if there was no pre-shower station in the test beam setup, isolating the calorimeter response. This results in an increased energy response and a reduced energy resolution, shown in Figure 9.

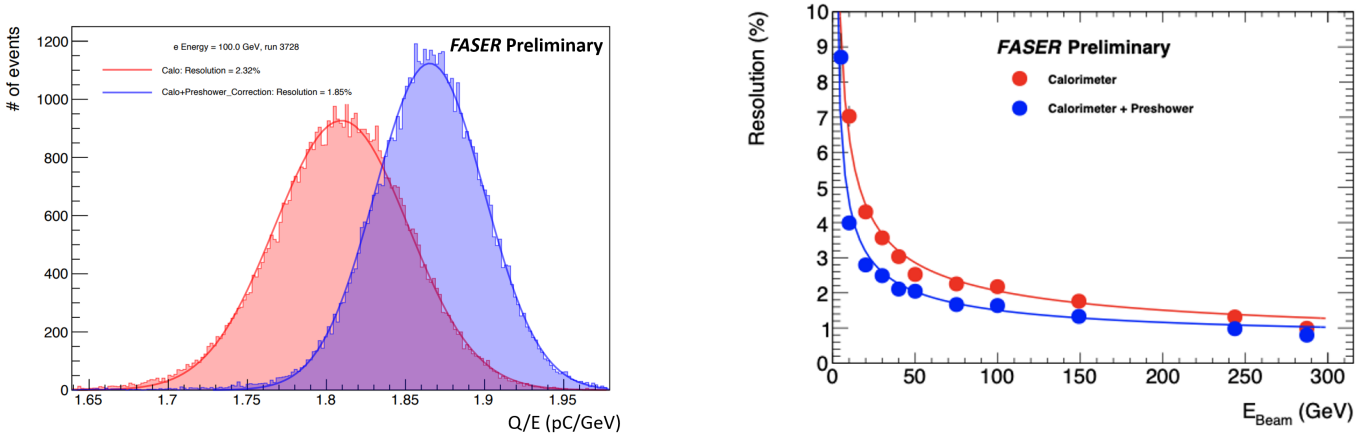

(**a**) (**b**)

Figure 9. (**a**) The change in deposited charge as a result of the pre-shower correction. (**b**) The improvement in energy resolution as a result of the pre-shower correction.

A version of the pre-shower correction must also be applied to the simulation, in order to correct the amount of deposited energy seen in the calorimeter. The deposited energy in the pre-shower versus calorimeter for a 100 GeV electron simulation is shown in Figure 10, as well as the equivalent plot with the correction applied. As with the test beam data, the correction gives an idea of the calorimeter response in the absence of a pre-shower station.

Data with the pre-shower material removed were taken to mimic a setup without the pre-shower station and evaluate as closely as possible the isolated calorimeter response. This effect was also studied in the simulation; the change in energy response from the removal of the tungsten and graphite material from the pre-shower station is shown in Figure 11.

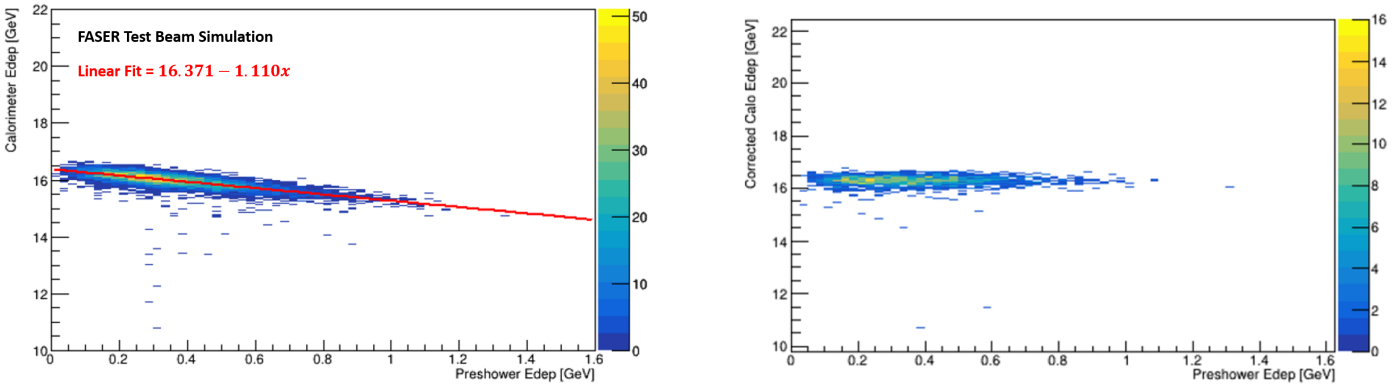

(**a**) (**b**)

Figure 10. The distribution of deposited energy in the pre-shower versus the calorimeter for a simulated 100 GeV electron (**a**) before and (**b**) after the pre-shower correction has been applied.

The simulation software was modified to compare with these data, removing the tungsten radiator and graphite from the simulation. The fraction of total energy deposited in the calorimeter increases from 15.5% to 16.4%. The change in the shape of the distribution was reflected by an improvement in energy resolution, shown in Table 1. There is good agreement between the quantative change in the energy resolution measurements with the pre-shower in place in the data, as summarised in Table 2. This effect is comparable to the application of the pre-shower correction in the data and simulation.

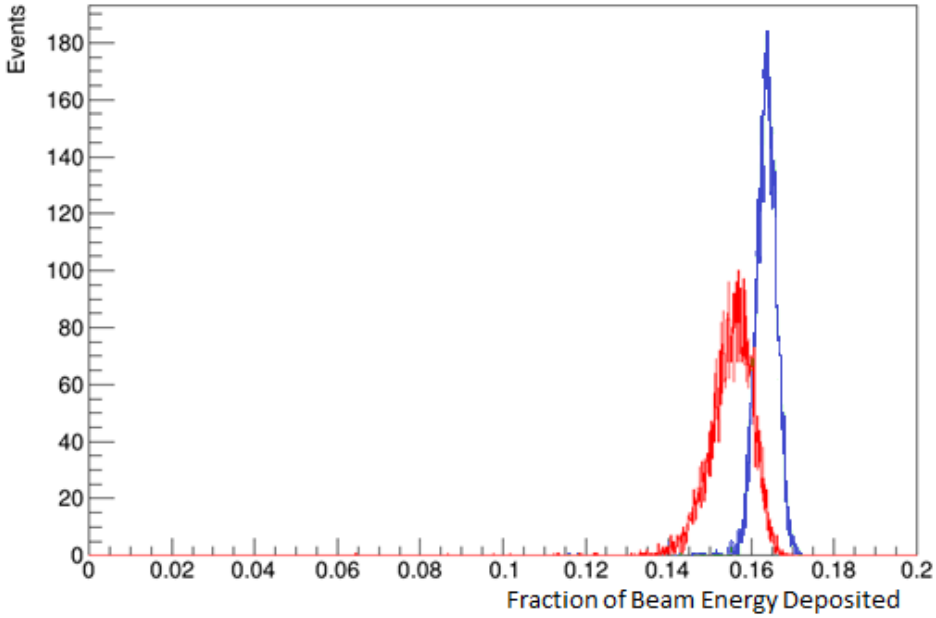

Figure 11. The fraction of beam energy deposited in the calorimeter for a simulated 30 GeV electron, with the tungsten/graphite material removed from the pre-shower station (blue), compared to the default simulation setup (red).

Table 1. Energy resolution measurements in test beam simulation at 2 different electron energies, with and without the pre-shower material.

Energy	With Pre-Shower	Tungsten/Graphite Removed
30 GeV	$2.72 \pm 0.04\%$	$1.58 \pm 0.02\%$
200 GeV	$0.9 \pm 0.01\%$	$0.71 \pm 0.01\%$

Table 2. Energy resolution measurements in test beam data at 2 different electron energies, with and without the pre-shower material.

Energy	With Pre-Shower	Tungsten/Graphite Removed
30 GeV	$3.76 \pm 0.03\%$	$2.84 \pm 0.02\%$
200 GeV	$1.89 \pm 0.01\%$	$1.67 \pm 0.01\%$

3.5. Energy Resolution

With the application of the pre-shower correction in both the test beam data and simulation, it is possible to compare the two, along with a parameterisation of the LHCb test beam results [10]. The calorimeter resolution as a function of electron energy is shown for 10 GeV–300 GeV in Figure 12.

Table 3 displays the energy resolution fit parameters. There is a difference in the a term in the data and simulation; the corrected simulation shows a lower value closer to that seen in the LHCb test beam. However, the addition of a noise term ($\frac{b}{E}$) vastly improves the fit in the case of data. This term was calculated from the measured noise of the digitiser signal. Since this term is related to the electronic noise of the readout chain, it was not included in the fit for the simulation. The simulation is also not able to accurately account for the constant term. Choosing a value of around 1%, in line with what LHCb measured, brings the higher energy end of the distribution upwards towards the test beam data; this is shown by the red fit in Figure 12. There are a number of factors that need to be considered before the differences in the energy response and energy resolution of the data and simulation can be fully understood, for example, the secondary effects discussed in Section 3.8. However, a resolution of 1–2% is more than sufficient for the next step of data analysis.

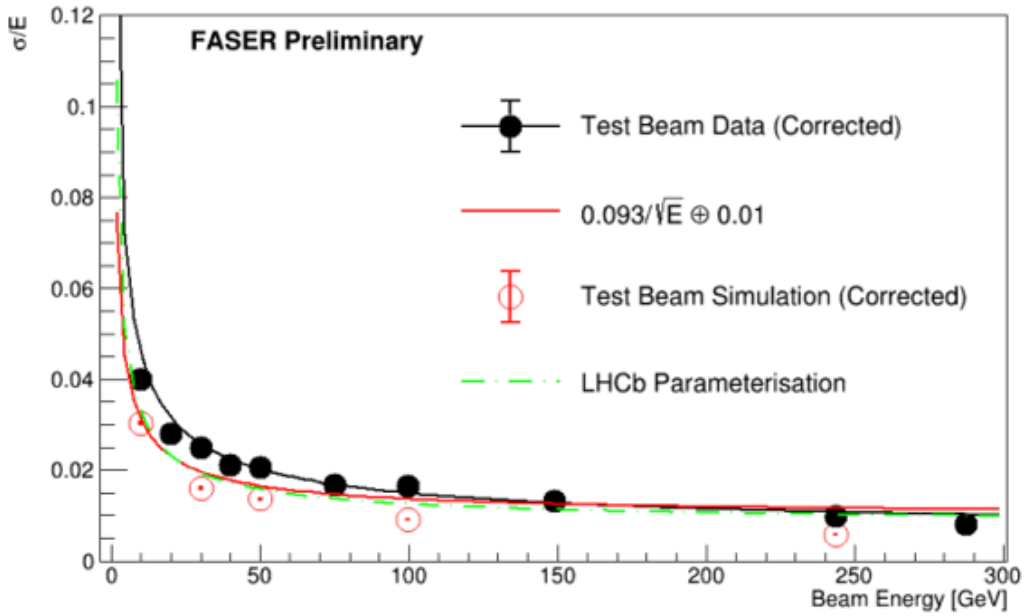

Figure 12. Energy resolution of the pre-shower corrected test beam data (black), the pre-shower corrected test beam simulation (red), and a parameterisation of LHCb test beam results using the same ECAL modules (green). The red line is a fit of the simulation points, with the addition of a 0.01 constant term.

Table 3. Calorimeter energy resolution values seen in Figure 12, including the fit used by LHCb, the corrected and uncorrected test beam data, and the corrected and uncorrected test beam simulation. Note that the test beam simulation does not include a noise term.

$\sigma_E/E = a/\sqrt{E} \oplus b/E \oplus c$			
	a	b	c
Data (Corrected)	0.134	0.151	0.0065
Data	0.196	0.151	0.0057
Simulation (Corrected)	0.093 ± 0.003	-	0.0000 ± 0.0004
Simulation	0.135 ± 0.001	-	0.0000 ± 0.0017
LHCb	0.094 ± 0.004	0.108 ± 0.029	0.0083 ± 0.0002

3.6. Energy Calibration

The data are in terms of the charge in pC divided by the beam energy, whereas the simulation is shown as a fraction of the beam energy. The deposits in the calorimeter from a 100 GeV electron are shown, in both the data and simulation, in Figure 13. The data and simulation from minimum ionising particles (MIPs) can be used to calibrate the response and convert from pC to GeV. The expected energy from the simulation can be estimated using the below relation:

$$\frac{Q(e^-)}{Q(\mu^-)} = \frac{E(e^-)}{E(\mu^-)}$$

where Q is the mean deposited charge in the calorimeter (from data), and E is the simulated mean deposited energy in the calorimeter, derived from crystal ball fits of the distribution in the case of electrons. For MIPs, the most probable value is derived from Landau fits of the distribution to account for the large tails. The pC to GeV conversion can be applied by considering the ratio of the charge deposited by an electron and the charge deposited by a MIP. Taking this ratio and scaling it according to the simulated energy deposition of an equivalent MIP signal gives an approximation of the energy, in GeV, deposited by such an electron. Comparison with Monte Carlo simulations allows for the extrapolation of other signal types. The resulting calculation showed that roughly 16.5% of beam energy

is deposited in the calorimeter; this can be seen in Figure 13b and agrees with predictions from simulations run prior to the test beam.

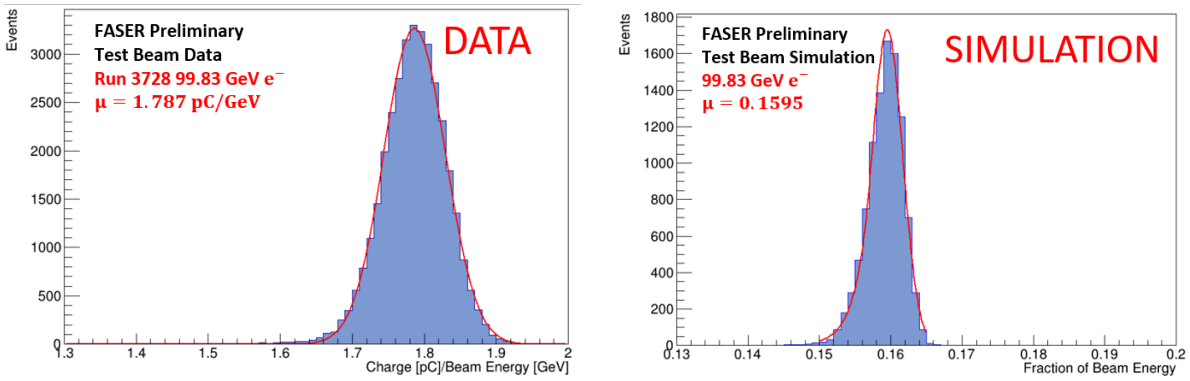

(**a**) (**b**)

Figure 13. (**a**) Deposited charge in the calorimeter for a 100 GeV test beam electron. (**b**) Deposited energy in the calorimeter for a simulated 100 GeV electron.

3.7. PID Capabilities

With the GeV conversion in place, it is possible to directly compare the data and simulation plots for the purpose of particle identification (PID). Here are example plots that show the signals of muons, pions, and electrons in the data and simulation in the pre-shower and in the calorimeter. The simulated signal from a 30 GeV electron, a 150 GeV muon, and a 200 GeV pion are shown in Figure 14. Plots derived from the test beam data for a 200 GeV electron, 150 GeV muon, and 200 GeV pion are shown in Figure 15. Exploring the PID capabilities of the pre-shower and calorimeter is important for understanding the potential to distinguish a signal from the background. Although the electron signal, particularly in the calorimeter, is distinct, it is likely to become more difficult to distinguish particle types at higher energies. When overlaid, there is a shift in the response between the data and simulation; further investigation is needed into the PID studies and energy calibration.

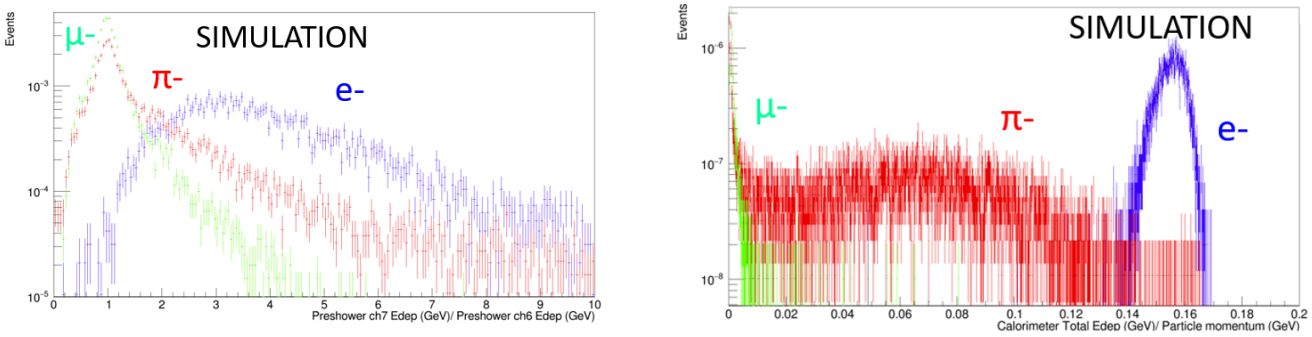

(**a**) (**b**)

Figure 14. Test beam simulation PID plots showing 200 GeV pion (green), 150 GeV muon (red), and 30 GeV electron (blue) simulated signals. (**a**) The ratio of deposited energy (GeV) in the two pre-shower station scintillator layers. (**b**) The ratio of deposited energy in the calorimeter and particle momentum (GeV).

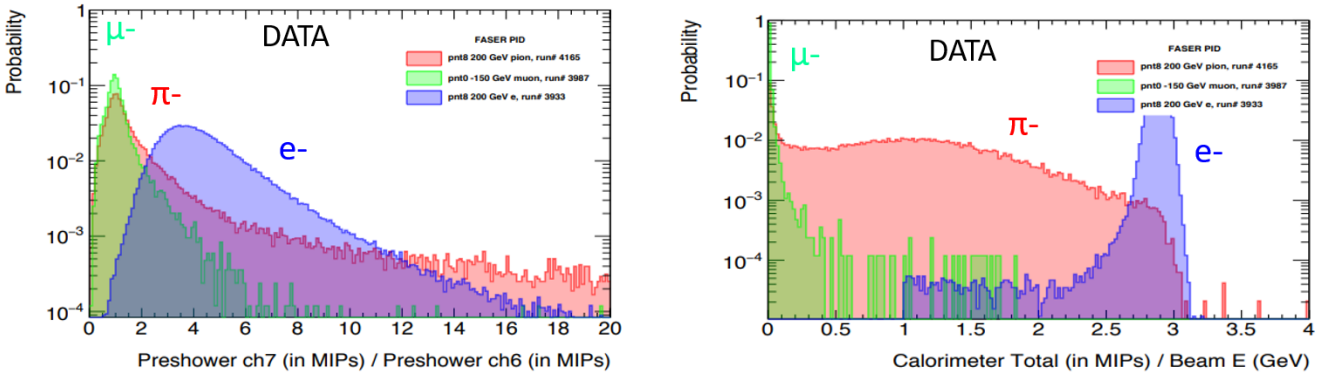

(**a**) (**b**)

Figure 15. Test beam data PID plots showing 200 GeV pion (green), 150 GeV muon (red), and 200 GeV electron (blue) simulated signal. (**a**) The ratio of deposited energy (GeV) in the two pre-shower station scintillator layers. (**b**) The ratio of deposited energy in the calorimeter and beam energy (GeV).

3.8. Local Calorimeter Effects

It was demonstrated in Section 3.5 that there are differences in the energy resolution fit between the simulation and data; the test beam was an opportunity to study effects in the calorimeter that may play a part in explaining these differences. One such observed effect was improvement in the light collection near wavelength shifting (WLS) optical fibres in the ECAL modules. LHCb set the amplitude of this effect to zero, and this had been coded into the simulation, but now it is possible to tune the specific amplitude based on the FASER test beam results. The calorimeter response as a function of the track position, fitted with a cosine function to extract an amplitude, is shown in Figure 16a. Another effect observed in the data was the increase in the generation of additional light, likely Cherenkov light, in the plastic light mixer in front of the PMT. This is seen when an MIP passes directly through a PMT in the calorimeter. This effect is illustrated in the heat map in Figure 16b.

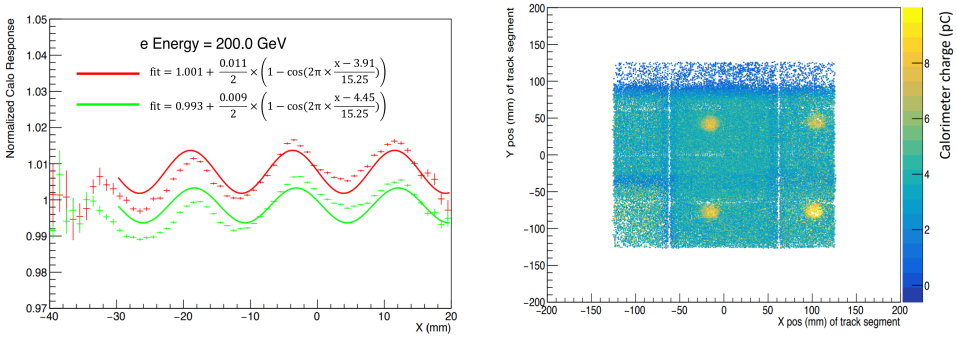

(**a**) (**b**)

Figure 16. (**a**) Measurement of improvement in light collection near WLS fibres made in the FASER test beam. The normalised calorimeter response as a function of the x position of the track segment is fit with a cosine function in order to extract the amplitude. (**b**) A heat map of the calorimeter, showing an increase in light deposits when an MIP travels through a PMT region.

4. Conclusions

In conclusion, the test beam saw efficient data taking with good overall beam quality and purity. The test beam results have been compared with the simulation, and energy calibration efforts are underway. In addition to this, the PID capabilities of the pre-shower and calorimeter are being studied. The energy response and resolution show generally good agreement between the data and simulation with some differences that are being investigated, and the energy resolution is sufficient for the next step of data analysis. The detector is once again situated in the TI12 tunnel, and the data taking for Run 3 has begun.

Funding: This research received no external funding.

Data Availability Statement: Not applicable

Acknowledgments: FASER is supported by CERN, the Simons Foundation, and the Heising-Simons Foundation.

Conflicts of Interest: The authors declare no conflict of interest.

Abbreviations

The following abbreviations are used in this manuscript:

FASER	Forward Search Experiment at the LHC	IFT	Interface Tracker
ALP	Axion-like Particle	ECAL	Electromagetic Calorimeter
LLP	Long-lived Particle	xAOD	Analysis Object Data
SM	Standard Model	ADC	Analogue to Digital Conversion
DS	Dark Sector	WLS	Wavelength Shifting Fibre
IP1	ATLAS Interaction Point	MIP	Minimum Ionising Particle
SCT	ATLAS Semiconductor Tracker	PMT	Photomultiplier Tube
PID	Particle Identification		

References

1. Ariga, A.; Abreu, H.; Mansour, E.A.; Antel, C.; Ariga, T.; Bernlochner, F.; Boeckh, T.; Boyd, J.; Brenner, L.; Cadoux, F.; et al. The FASER Detector. CERN-FASER-2022-001. *arXiv* **2022**, arXiv:2207.11427.
2. Ariga, A.; Ariga, T.; Boyd, J.; Cadoux, F.; Casper, D.W.; Favre, Y.; Feng, J.L.; Ferrere, D.; Galon, I.; Gonzalez-Sevilla, S.; et al. *Technical Proposal: FASER, the Forward Search Experiment at the LHC*; Tech. Rep. CERN-LHCC-2018-036. LHCC-P-013; CERN: Geneva, Switzerland, 14 December 2018. Available online: http://cds.cern.ch/record/2651328 (accessed on 24 July 2022).
3. Ariga, A.; Ariga, T.; Boyd, J.; Cadoux, F.; Casper, D.W.; Favre, Y.; Feng, J.L.; Ferrere, D.; Galon, I.; Gonzalez-Sevilla, S.; et al. FASER's Physics Reach for Long-lived Particles. *Phys. Rev. D* **2019**, *99*, 095011. [CrossRef]
4. Battaglieri, M.; Belloni, A.; Chou, A.; Cushman, P.; Echenard, B.; Essig, R.; Estrada, J.; Feng, J.L.; Flaugher, B.; Fox, P.J.; et al. US Cosmic Visions: New Ideas in Dark Matter 2017: Community Report. *arXiv* **2017**, arXiv:1707.04591.
5. Abdesselam, A.; Akimoto, T.; Allport, P.P.; Alonso, J.; Anderson, B.; Andricek, L.; Anghinolfi, F.; Apsimon, R.J.; Barbier, G.; MacWaters, C.; et al. The barrel modules of the ATLAS semiconductor tracker. *Nucl. Instrum. Meth. A* **2006**, *568*, 642–671. [CrossRef]
6. LHCb Collaboration. *LHCb Calorimeters: Technical Design Report*; CERN: Geneva, Switzerland, 2000. Available online: http://cds.cern.ch/record/494264 (accessed on 24 July 2022).
7. H2 Beam Line. Available online: http://sba.web.cern.ch/sba/BeamsAndAreas/H2/H2_presentation.html (accessed on 24 July 2022).
8. Geant4 Collaboration. CERN. Available online: https://geant4.web.cern.ch/ (accessed on 24 July 2022).
9. ATLAS Collaboration. The VP1 ATLAS 3D Event Display. Available online: http://atlas-vp1.web.cern.ch/ (accessed on 24 July 2022).
10. Arefev, A.; Kvaratskheliia, T.; Morozov, A.; Melnikov, E.; Voronchev, K.; Roussinov, D.; Barsuk, S.; Belyaev, I.; Bobchencko, B.; Martemyanov, M.; et al. *Beam Test Results of the LHCb Electromagnetic Calorimeter*; CERN-LHCB-2007-149; CERN: Geneva, Switzerland, 2008.